Supplemental Information

In-situ molecular compensation in wide-bandgap perovskite for efficient all-perovskite tandem solar cells

Sheng Fu,*[a+] Nannan Sun,[a+] Shuaifeng Hu,[b+] Hao Chen,*[c] Xinxin Jiang,[d] Yunfei Li,[a] Xiaotian Zhu,[a] Xuemin Guo,[a] Wenxiao Zhang,[a] Xiaodong Li,[a] Andrey S. Vasenko,[d] and Junfeng Fang*[a]

[a.]School of Physics and Electronic Science, Engineering Research Center of Nano-photonics and Advanced Instrument Ministry of Education, East China Normal University, Shanghai 200062, China.
E-mail: sfu@phy.ecnu.edu.cn, jffang@phy.ecnu.edu.cn

[b.]Clarendon Laboratory, Department of Physics, University of Oxford, Oxford OX1 3PU, UK.

[c.]Global Institute of Future Technology (GIFT), Shanghai Jiao Tong University, Shanghai 200240, China.
E-mail: hao.chen1@sjtu.edu.cn

[d.]HSE University, Moscow 101000, Russia

[+]These authors contribute equally to this work

Experimental Part

Materials and precursor fabrications

The halide salts for perovskite fabrications were ordered from Xi'an Yuri Solar, including FAI, MAI, MACl, PbI_2, 5-AVAI, $PbBr_2$ and $PbCl_2$. The KSCN, SnI_2, EDA as well as the solvents (DMF, DMSO, IPA, DI water, anhydrous ethanol Et-OH, Anisole and Chlorobenzene CB) were bought from Sigma. The PEDOT:PSS (Al 4083) was purchased from Heraeus Clevios (Germany). The Me-4PACz, BCP and $PDAI_2$ were provided by TCI. The C_{60} powders, SnF_2, PCBM and NiOx nanoparticles were obtained from Advanced Election Technology. The metal sources of Ag and Au were provided by the ZhongNuo Advanced Material (Beijing)Technology Co., Ltd. The raw materials were directly used without further purification.

The precursors with the chemical compound of $FA_{0.8}Cs_{0.2}PbI_{1.8}Br_{1.2}$ were prepared by dissolving CsI:FAI:PbI_2:$PbBr_2$=0.2:0.8:0.4:0.6 in 1 mL mixture DMF/DMSO (volume ratio of 4:1) solvent with the molar concentration of 1.2 M without heating. 5% $MAPbCl_3$ (4.05 mg MACl+16.65 mg $PbCl_2$) and 2 mg KSCN as additives were introduced into the precursor for superior crystallization. The 5-AVAI was directly incorporated into the precursor with a concentration of 1.5 mg/mL. The precursor should be filtered with 0.22 μm PTFE membrane before use. The precursors of low-bandgap perovskite were prepared as same as previous report with the chemical formula of $Cs_{0.05}MA_{0.25}FA_{0.7}Pb_{0.5}Sn_{0.5}I_3$ with the molar concentration of 1.8 M in the DMF/DMSO (3:1) solvent.[1] 5 mg Pb powders were used to reduce the Sn^{4+} amounts. NiO_X NPs were dispersed in the DI water with a concentration of 10 mg/mL. $PDAI_2$ was dissolved in IPA (1 mg/mL) as surface passivation for WBG perovskite. Me-4PACZ solutions were prepared with 0.5 mg/mL in Et-OH. PEDOT: PSS for tandem devices was diluted by 3 times with IPA. EDA acting as the surface passivation for LBG perovskite was 0.05 mg/mL in CB.

Solar cell fabrications

The ITO substrates were ultrasonically cleaned in the order of detergent, water, acetone and IPA for 20 min for each step. The dried ITO substrates were exposed to UV ozone for 20 min for further cleaning and good wettability. NiO_X NPs were spin-coated on ITO at 4000 rpm (acceleration rate of 2000) for 30 s at ambient conditions. Then, the Me-4PACz was coated on the NiO_X at 3500 rpm for 30 s, following 100 ^oC annealing for 10 min. After cooling down, the perovskite films were coated with the procedure of 1000 rpm for 5 s and 3500 rpm for 28 s, and anti-solvent treatment with 100 μL anisole was used at 10 s before the end. The wet perovskite films were put on 105 ^oC hotplate to anneal for 15 min. After that, surface passivation with $PDAI_2$ (dynamically coated) was performed at 4500 rpm for 30 s with further annealing at 100 ^oC for 5 min. The substrates were transferred into a vacuum chamber to evaporate 30 nm C_{60} (deposition rate around 0.15 Å/s), and then put into ALD chamber to deposit 25 nm ALD-SnO_2. 120 nm silver (Ag) was evaporated on the ALD SnO_2 with a speed of around 0.3 Å/s under the mask with an aperture area of 0.073 (defined by the overlapping zoon of ITO and Ag). For All-perovskite tandem devices fabrications, the processes were same as the WBG perovskite fabrications to ALD deposition. 1 nm Au were thermally evaporated on ALD-SnO_2. The diluted PEDOT:PSS solution were coated on the substrates at 3500 rpm for 30 s and transferred into glovebox after annealing at 120 ^oC for 10 min. The LBG perovskite films were coated with 2-step procedure: 1000 rpm for 10 s and 3500 rpm for 40 s. 400 μL CB as antisolvent was applied at the 20^{th} s of the second step, following 100 ^oC annealing for 10 min to complete the crystallization and phase transition. The EDA surface treatment was taken on the cold perovskite at 4000 rpm for 30 s, and annealed at 100 ^oC for 8 min. Then, the substrates were moved into evaporation chamber to deposit 25 nm C_{60}, 6 nm BCP and 130 nm Ag.

Characterizations

The J-V curves of WBG and tandem PSCs were collected on the solar simulator with AM 1.5 100 mW/cm^2 illumination with data recording by the Keithley 2400 source meter. The sweep voltage range was from -0.2 to 1.5 V in a step of 0.15 V/s with a

dwell time of 40 ms, and the range for tandem devices was -0.2-2.25 V. The EQE spectra of the solar cells were measured with the model IVQE8-C system. The spectra of the AM1.5 simulator and EQE light source were calibrated by the standard Si cell certified by Newport. For tandems, the lamps of 530 nm and 950 nm were used to measure the EQE responses of bottom and top cells, respectively. The TPC and TPV measurements of the WBG PSCs were conducted on the electrochemical workstation (Solartorn 1260A impedance analyser). The light intensity dependence of the devices was taken on the simulator and the light intensity was calculated based on the performance of the standard Si cell. The top-view and cross-section SEM images of films and devices were captured on the Zeiss GeminiSEM450 at the operational voltage of 4 kV. The AFM and KPFM images of the samples were collected on Dimension 3100, where the mode for KPFM measurements was set as voltage equal to work function (WF) perovskite surface reducing WF of the tip. The XPS spectra of both SAMs and perovskite films were obtained from the Kratos AXIS ULTRA. TOF-SIMS of the perovskite films were conducted on the TOF–SIMS 5 IONTOF with the Cs source in 1 KV voltage. The PL and TRPL measurements were performed on the Fluorolog-Horiba system and Delta Flex Fluorescence Lifetime System. The H^1NMR($(CD_3)_2SO$, 400 MHz AVANCE III) and FTIR (neaSNOM-nanoFTIR||1) measurements were conducted to identify the interaction between 5-AVAI and perovskite. The hyperspectral PL mappings were recorded by the inVia Reflex (Renishaw, UK) under 1 sun 532-nm laser-illuminated, and the PL peaks of different ageing times were the highest PL emission ones. The UV-vis absorption of the films and solutions was taken on the PerkinElmer Lambda 1050. The I_2 emission was quantified by putting the perovskite (infused in the CB) on 85 ^oC hotplate under 1 sun illumination. The EL of the devices was collected at the Enlitech REPS-Pro system with the Voltage scanning from 1.4 to 1.8 V, and the EL signals were recorded by a Si-Ge alloying sensor in a dark box without integral sphere.

DFT simulations

All first-principles calculations in this work were performed with Density-functional

theory (DFT) as implemented in the Vienna Ab initio Simulation Package (VASP) code.[2-4] The generalized gradient approximation (GGA) of the Perdew−Burke−Ernzerhof (PBE) functional was used to treat the exchange-correlation potential.[50] A plane-wave energy cutoff of 550 eV and a Γ-centered 3 × 3 × 1 k-point mesh was used for geometry optimizations. All atomic coordinates were relaxed until the total energy converges below 10^{-4} eV and 0.02 eV/Å for force were reached. A 20 Å vacuum layer was added along the z direction to eliminate interactions between adjacent slabs.

To quantitatively evaluate the stability of the adsorption system, the adsorption energies (E_{ads}) are defined as, $E_{ads} = E_{mol/sub} - E_{mol} - E_{sub}$, where $E_{mol/sub}$ is the total energies of the adsorbed system, E_{mol} is the energy of isolated molecules (5-AVAI and Me-4PACZ), and E_{sub} is the total energies of clean NiO_X substrate.

Stability evaluations: The MPPT of both single-junction and tandem devices were taken under simulated 1-sun illumination at ambient conditions. The device surface temperature was around 35 ºC. All devices were encapsulated by UV epoxy (UV Adhesive LT-U001, UV curing for 3 min) in the glovebox before use.

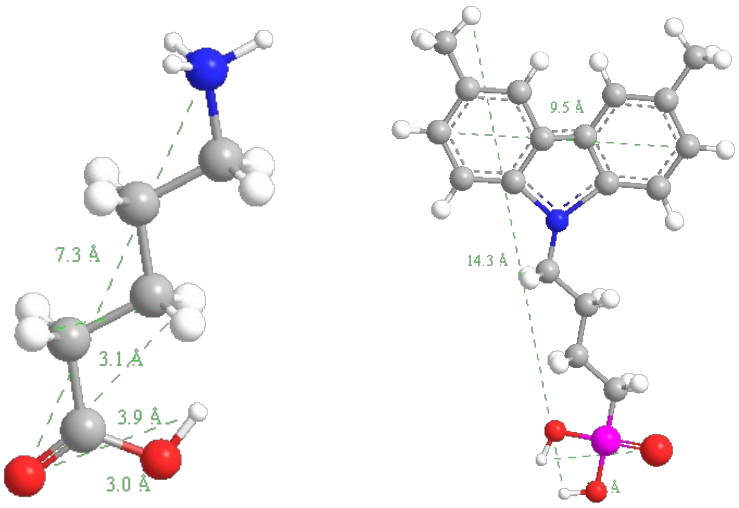

Fig. S1. Theoretical calculations on the molecular size of 5-AVAI and Me-4PACz.

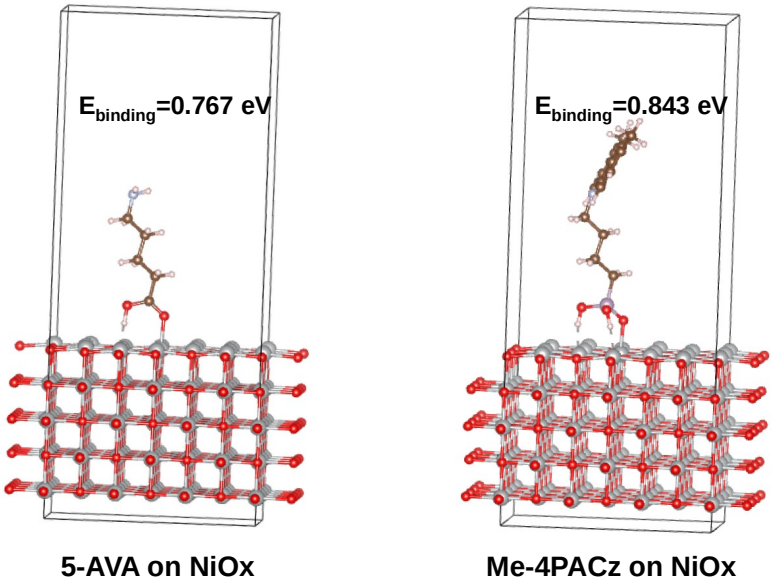

Fig. S2. Geographic diagrams of the DFT results for molecule bonding on NiOx surface.

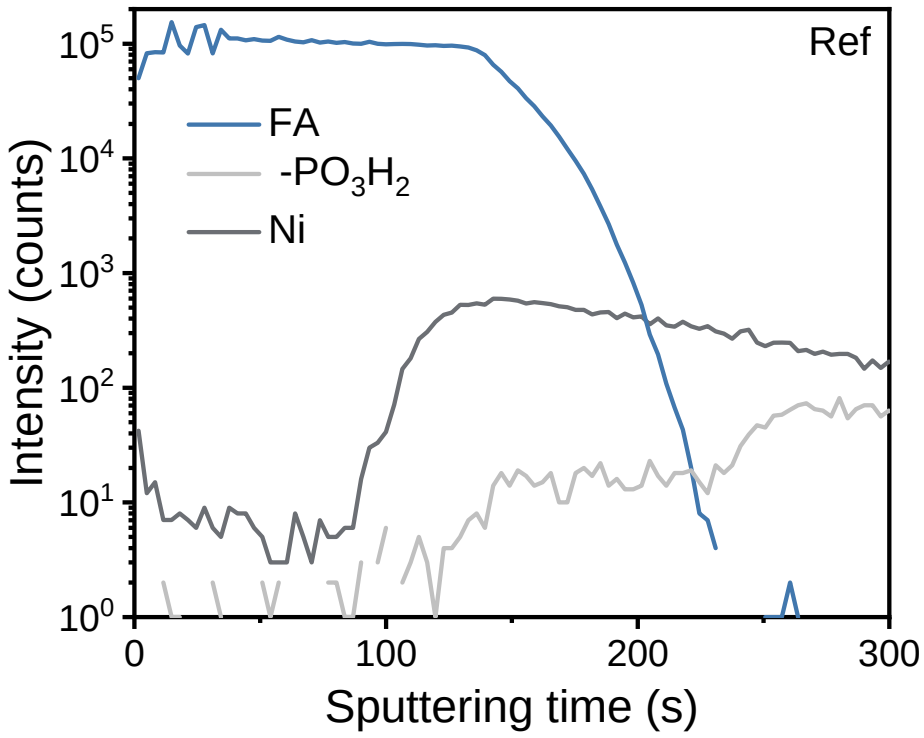

Fig. S3. ToF-SIMS result on the Ref film.

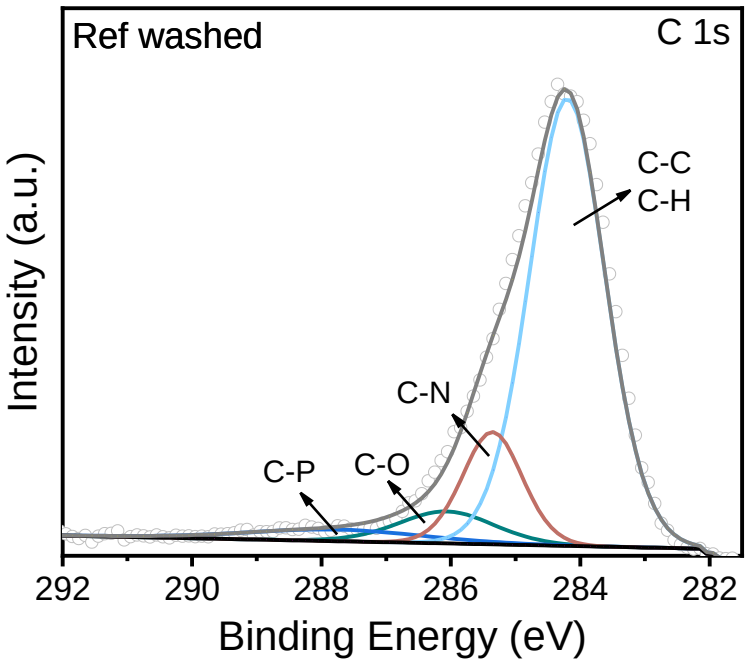

Fig. S4. C 1s XPS spectra of the Ref perovskite film after DMF washed.

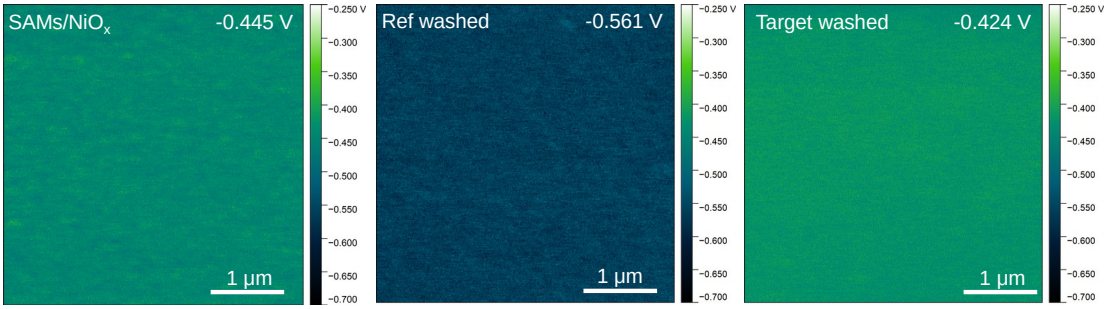

Fig. S5. Raw KPFM images of the Ref and Target WBG perovskite films after DMF washed.

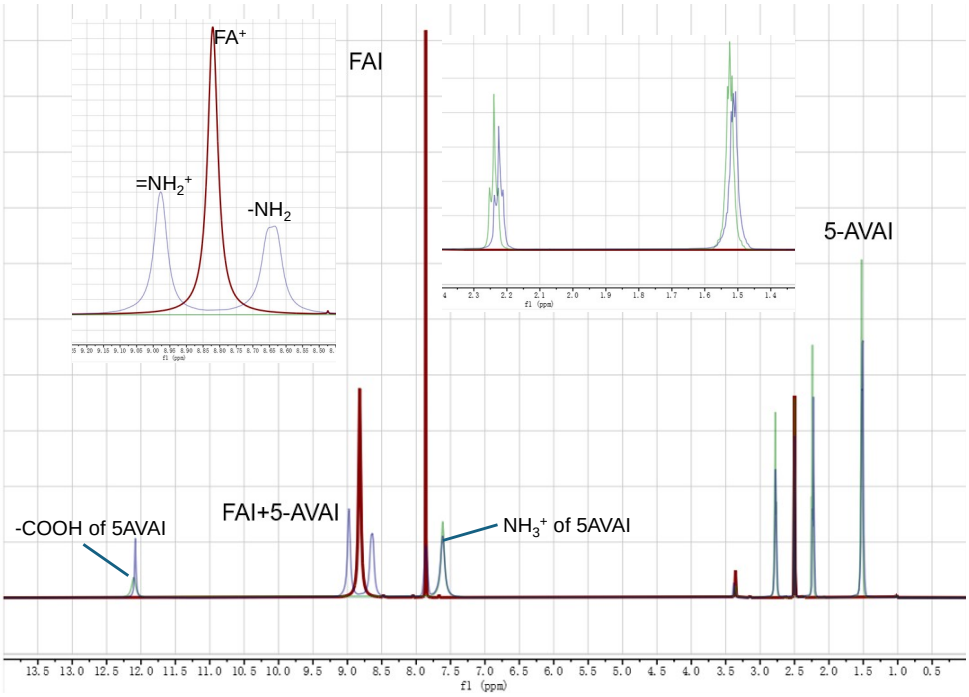

Fig. S6. H^1MNR of the FAI (red), 5-AVAI (green) and FAI@5-AVAI (purple). After mixing these two powers in d6MSO, the obvious chemical shift can be detected (as the insets), corresponding to the strong hydrogen bindings. Compared to the shifts of the –COOH and $–NH_3^+$ signals in 5-AVAI, the –COOH group exhibits a more pronounced change, suggesting that hydrogen bonding with FA is primarily mediated by the –COOH group.

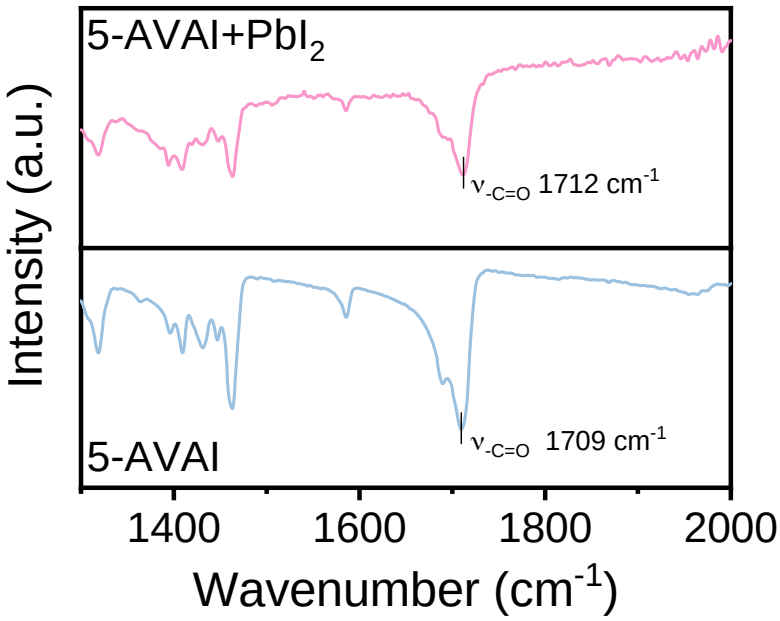

Fig. S7. FTIR spectra of pure 5-AVAI and 5-AVAI+PbI_2. The -C=O signal is shifted from 1709 to 1712 cm^{-1} after mixing with PbI_2, indicating to the formation of coordination bindings.

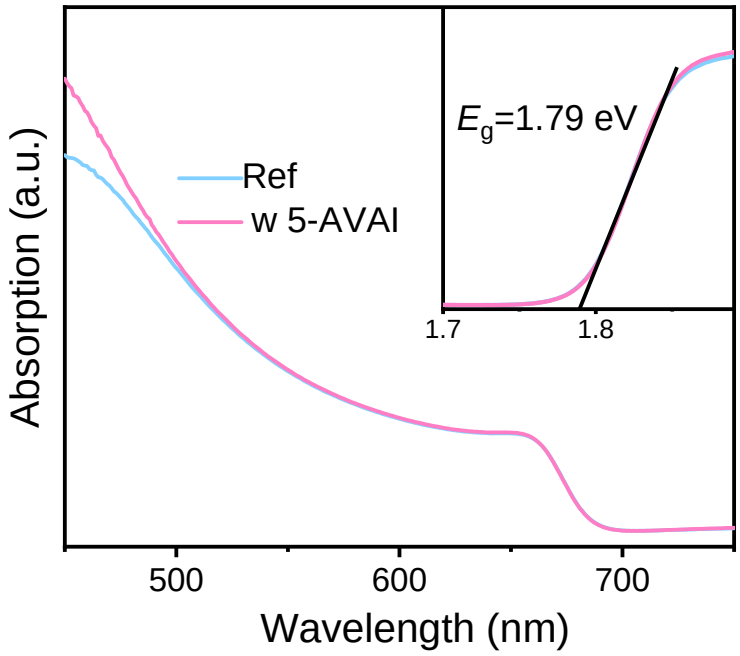

Fig. S8. UV-vis absorption and the fitting results of the Ref and target WBG perovskite films.

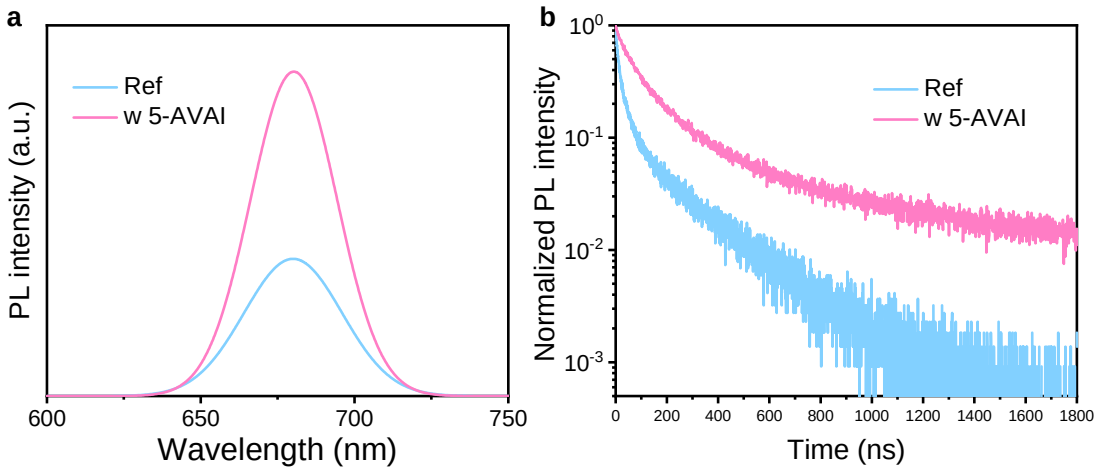

Fig. S9. PL (a) and TRPL curves of the Ref and Target WBG perovskite films.

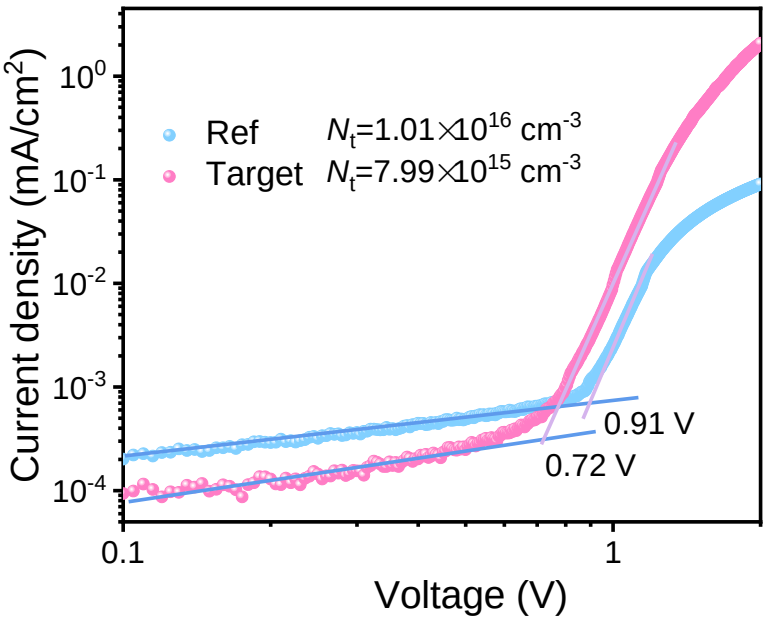

Fig. S10. SCLC curves and the corresponding trap density for the Ref and target films. A hole-only configuration of ITO/NiO_x/Me-4PACz/PVK/PTAA/Au was used for SCLC evaluation.

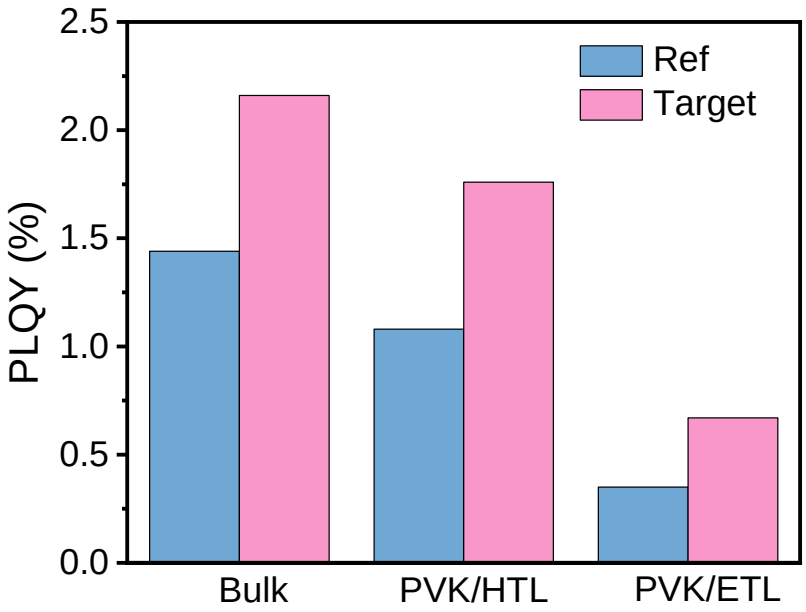

Fig. S11. PLQY values of the Ref and target films. The signals were collected from PVK/glass (bulk), PVK/HTL (from glass side) and PVK/ETL (from film side).

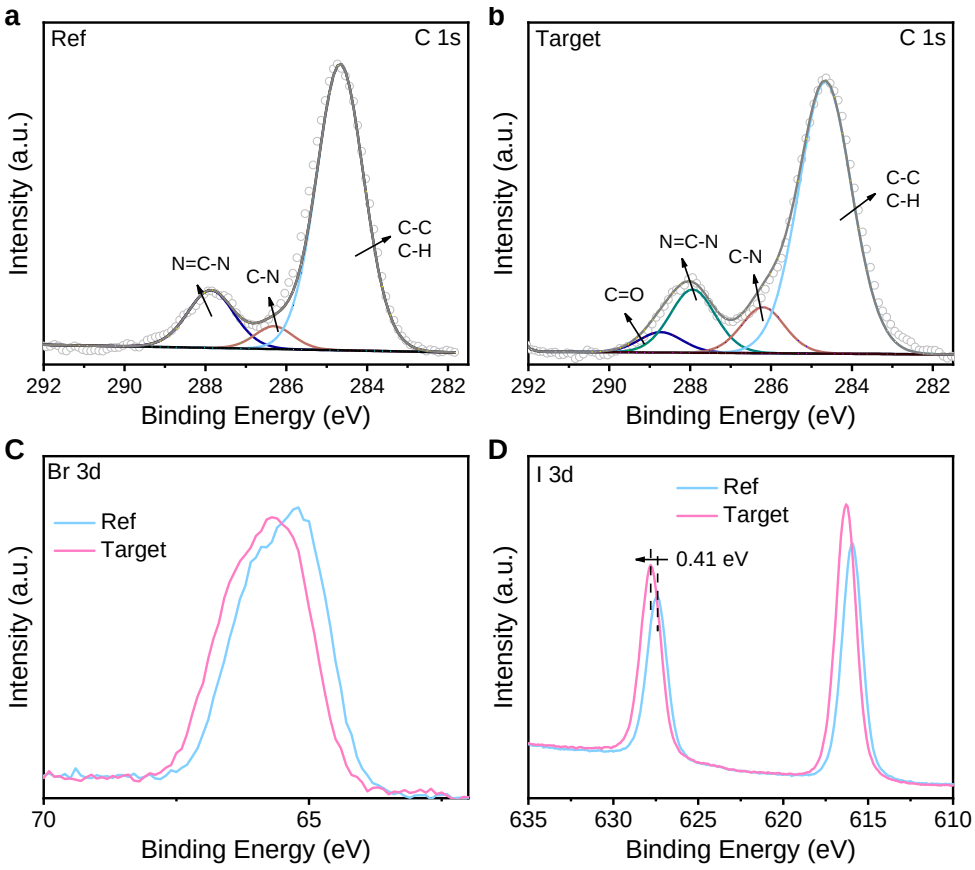

Fig. S12. C 1s, Br 3d and I 3d XPS spectra of the Ref and Target WBG perovskite

films.

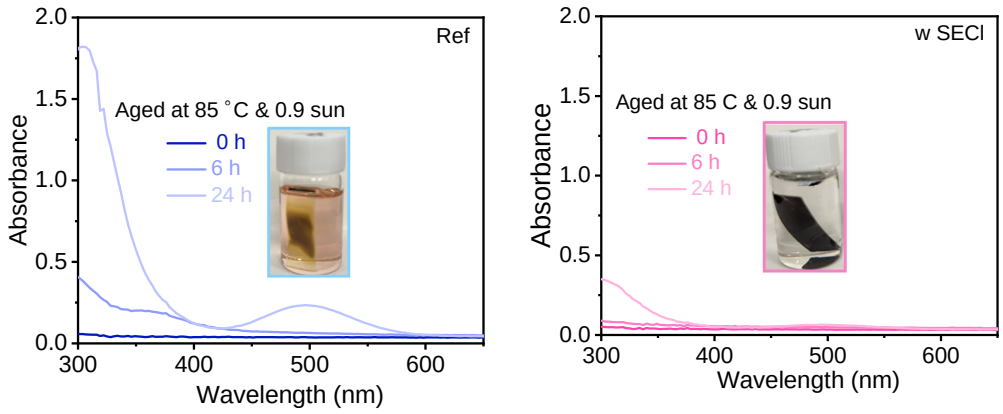
Ref
Aged at 85 ˚C & 0.9 sun
0 h
6 h
24 h
Absorbance
Wavelength (nm)
w SECl
Aged at 85 C & 0.9 sun
0 h
6 h
24 h
Absorbance
Wavelength (nm)

Fig. S13. UV-vis absorption spectra of the Ref (a) and Target (b) films soaking in the toluene under 0.9-sun white LED illumination at 85 ºC hotplate for different aging time.

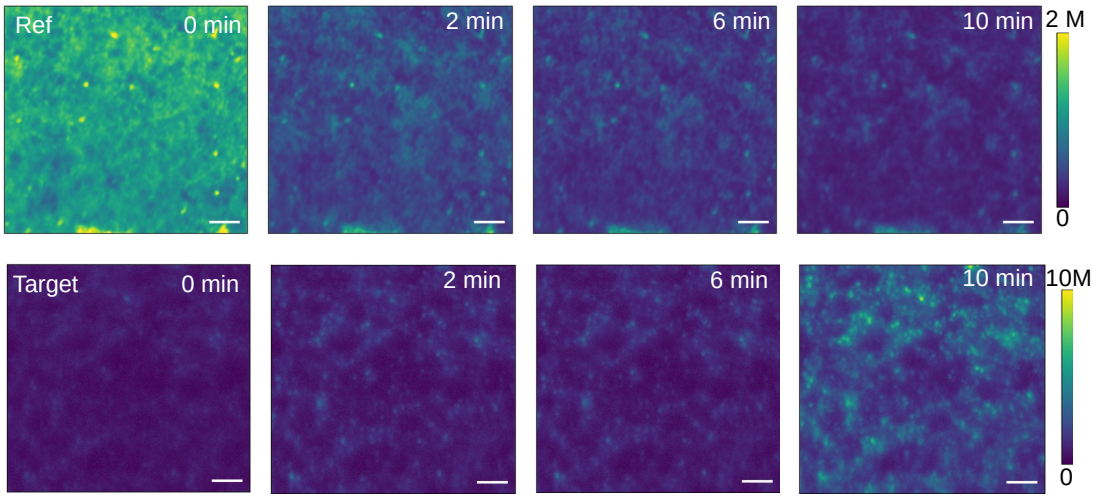

Fig. S14. Light soaking ages of the Ref and Target films for different time. The inset bar is 20 μm.

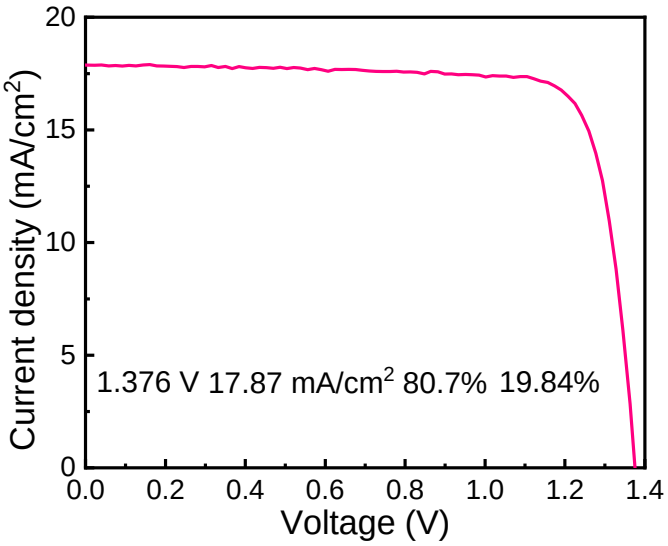

Fig. S15. J-V curve of the Target device with the highest V_{OC} of 1.376 V.

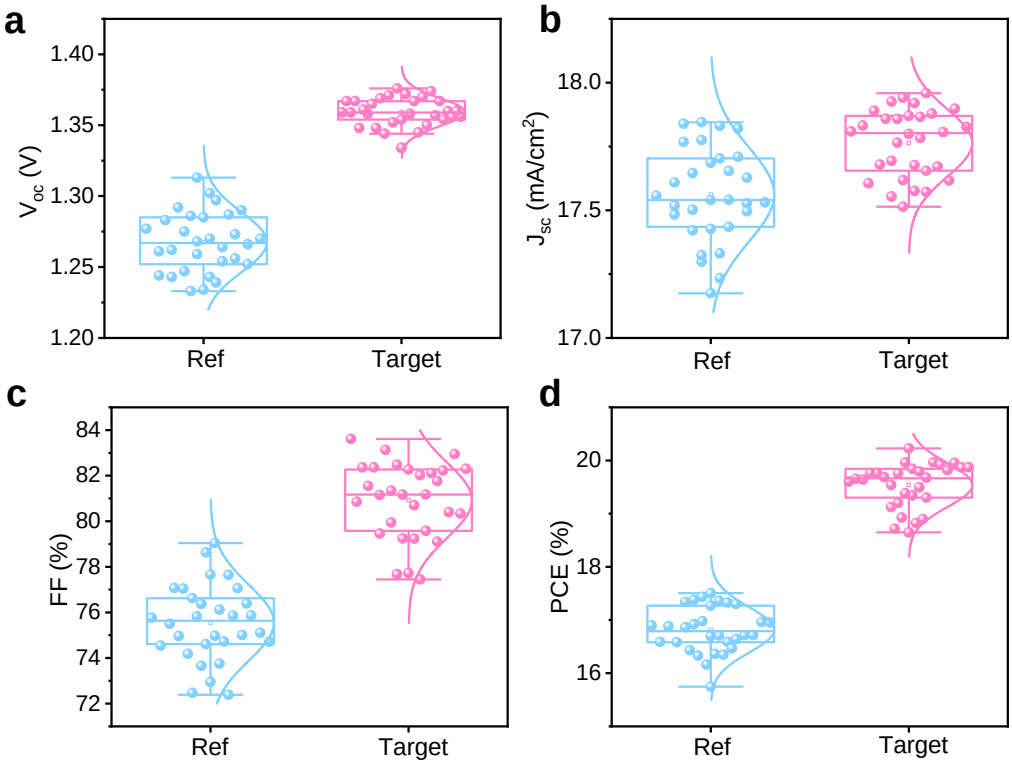

Fig. S16. Photovoltaic parameters statistics of V_{OC} (a), J_{SC} (b), FF (c) and PCE (d) of the Ref and Target WBG PSCs.

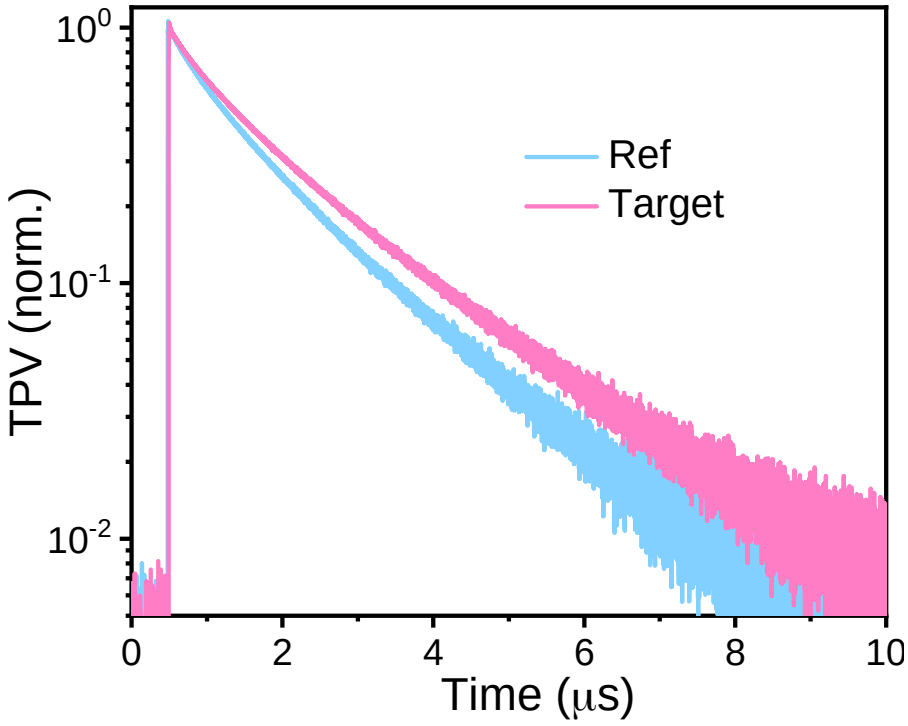
TPV (norm.)
10^0
10^{-1}
10^{-2}
0
2
4
6
8
10
Time (μs)
Ref
Target

Fig. S17. TPV curves of the Ref and Target WBG PSCs.

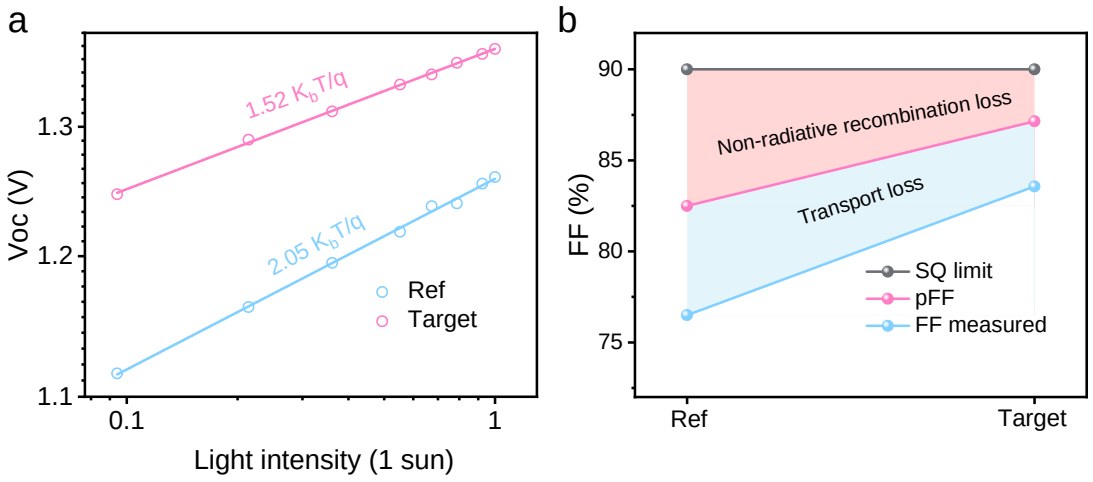

Fig. S18. V_{OC}-light intensity dependence (a) and FF loss analysis (b) of the Ref and Target devices.

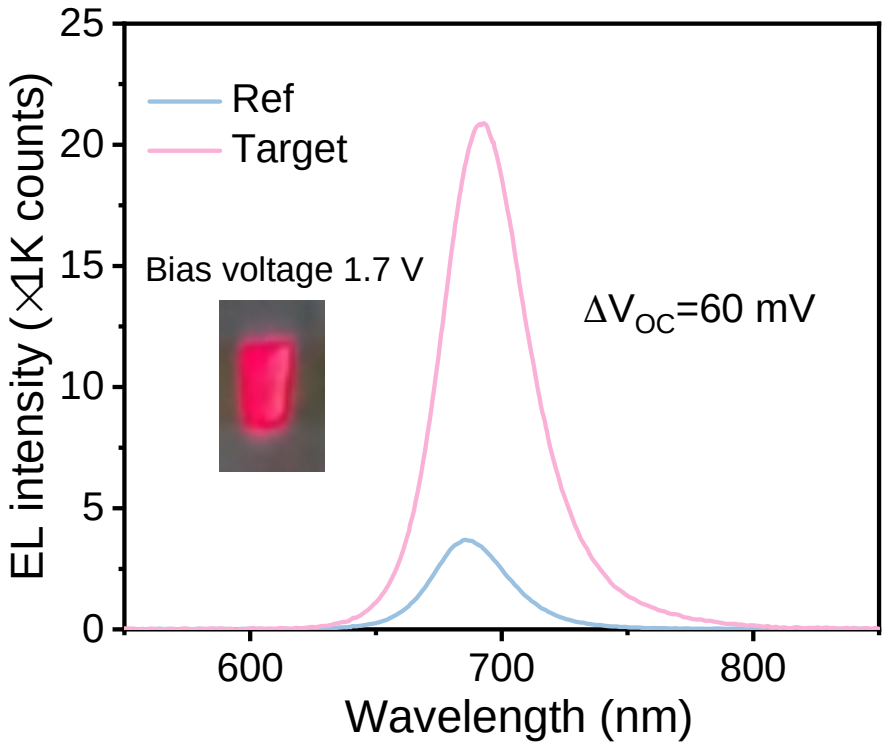

Fig. S19. EL curves of the WBG PSCs under bias of 1.7 V and the inset is the EL image. The fitted V_{OC} change is around 60 mV, lower than the measured ΔV_{OC} (87 mV). There is no integrated sphere during EL measurement, which leads to a higher error (loss) with higher EL efficiency.

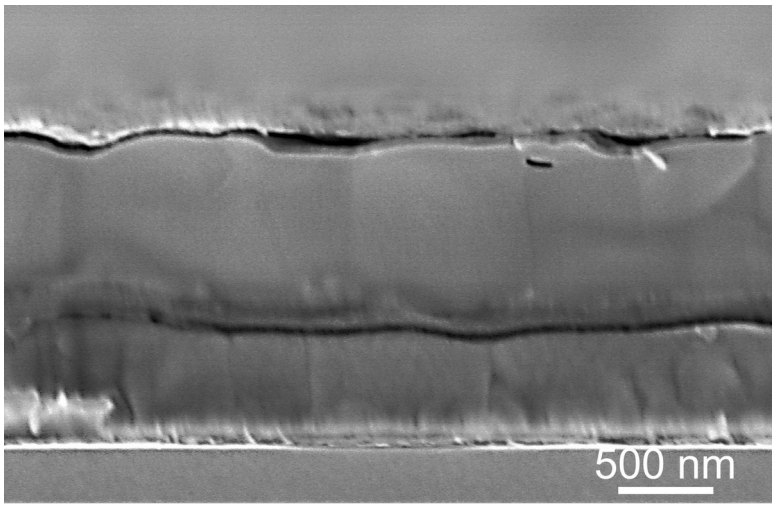

Fig. S20. Cross-section SEM image of the APTSCs.

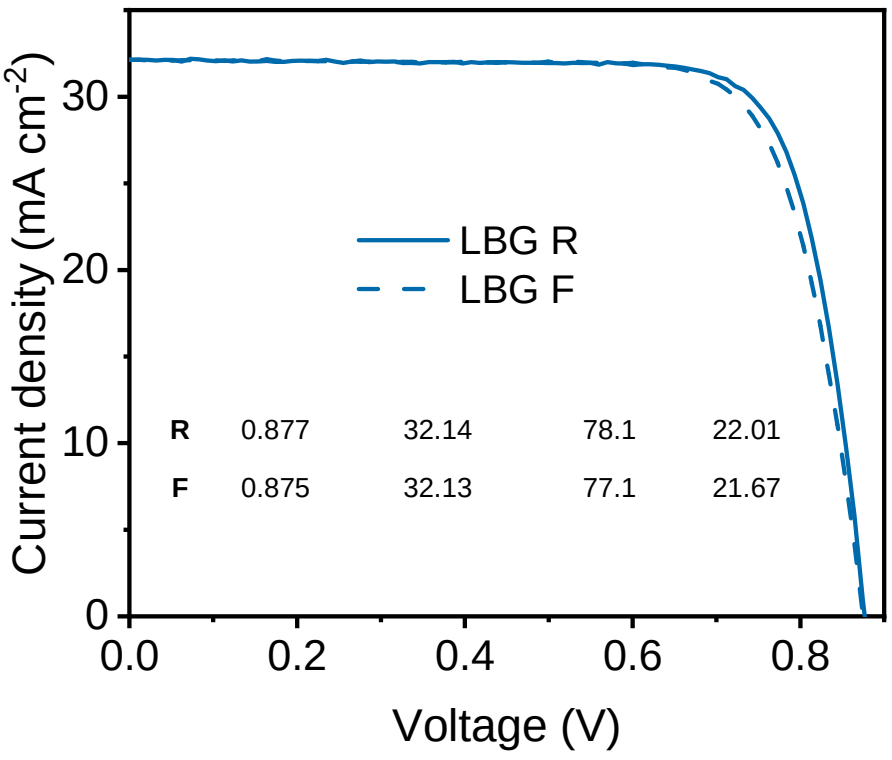

Fig. S21. J-V curves of the LBG perovskite subcell used in APTSCs.

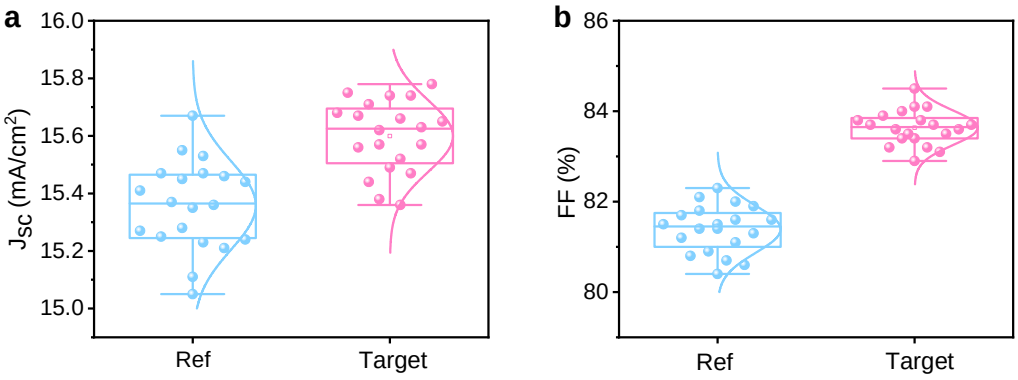

Fig. S22. Photovoltaic parameters statistics of JSC (a) FF (b) of the Ref and Target APTSCs.

Table S1. Reported high-efficiency WBG PSCs for APTSCs and the detailed parameters.

Eg /eV	V_{OC}/V	PCE/%	V_{OC} deficit/V	PCE for tandems/%	Ref
1.76	1.22	17.3	0.54	26.4	Tan[5]
1.78	1.23	16	0.55	24.4	Huang[6]
1.77	1.34	20.37	0.43	27.04	Ning[7]
1.79	1.33	20.3	0.46	27	Sargent[8]
1.77	1.23	18.5	0.54	25.6	Tan[9]
1.78	1.32	19.6	0.46	28.1	Tan[10]
1.81	1.35	19.58	0.46	25.22	Jen[11]
1.75	1.33	20.1	0.42	27.1	Jiang[12]
1.77	1.31	19.3	0.46	27.22	Zhao[13]
1.77	1.31	18.46	0.46	27	Zhao[14]
1.77	1.35	20.5	0.42	28.5	Tan[15]
1.77	1.30	19.53	0.47	28.8	Chen[16]
1.8	1.32	18.92	0.48	25.8	Li[17]
1.88	1.36	18.3	0.52	26.4	Li[18]
1.79	**1.376**	**20.23**	**0.414**	**28.9**	**Our**

Table S2. Photovoltaic parameters of the Ref and Target WBG PSCs and APTSCs.

	Scan direction	**V_{OC} (V)**	**J_{SC} (mA cm^{-2})**	**FF (%)**	**PCE (%)**
Ref WBG	Forward	1.28	17.77	74.97	17.05
	Reverse	1.285	17.54	77.66	17.50
Average		1.268±0.021	17.56±0.18	75.55±1.66	16.82±0.43
Target WBG	Forward	1.37	17.93	81.37	19.99
	Reverse	1.372	17.92	82.27	20.23
Average		1.359±0.010	17.76±0.13	80.92±1.65	19.54±0.42
Ref APTSCs	Forward	2.113	15.50	81.2	26.59
	Reverse	2.128	15.53	82.3	27.20
Average		2.080±0.030	15.36±0.15	81.4±0.5	26.00±0.48
Target APTSCs	Forward	2.182	15.72	83.0	28.47
	Reverse	2.183	15.74	84.1	28.90
Average		2.158±0.021	15.60±0.12	83.6±0.4	28.15±0.46

References

1. L. Chen, C. Li, Y. Xian, S. Fu, A. Abudulimu, D. B. Li, J. D. Friedl, Y. Li, S. Neupane, M. S. Tumusange, N. Sun, X. Wang, R. J. Ellingson, M. J. Heben, N. J. Podraza, Z. Song, Y. Yan, *Adv. Energy Mater.* 2023, **13**, 202301218.

2. S. Goedecker, M. Teter, J. Hutter, *Phys. Rev. B* 1996, **54**, 1703.

3. J. P. Perdew, K. Burke, M. Ernzerhof, *Phys. Rev. Lett.* 1996, **77**, 3865.

4. S. Grimme, J. Antony, S. Ehrlich, H. Krieg, *J. Chem. Phys.* 2010, **132**, 154104.

5. R. Lin, J. Xu, M. Wei, Y. Wang, Z. Qin, Z. Liu, J. Wu, K. Xiao, B. Chen, S. M. Park, G. Chen, H. R. Atapattu, K. R. Graham, J. Xu, J. Zhu, L. Li, C. Zhang, E. H. Sargent, H. Tan, *Nature* 2022, **603**, 73.

6. Z. Yu, Z. Yang, Z. Ni, Y. Shao, B. Chen, Y. Lin, H. Wei, Z. J. Yu, Z. Holman, J. Huang, *Nat. Energy* 2020, **5**, 657.

7. X. Jiang, Q. Zhou, Y. Lu, H. Liang, W. Li, Q. Wei, M. Pan, X. Wen, X. Wang, W. Zhou, D. Yu, H. Wang, N. Yin, H. Chen, H. Li, T. Pan, M. Ma, G. Liu, W. Zhou, Z. Su, Q. Chen, F. Fan, F. Zheng, X. Gao, Q. Ji, Z. Ning, *Natl. Sci. Rev.* 2024, **11**, nwae055.

8. H. Chen, A. Maxwell, C. Li, S. Teale, B. Chen, T. Zhu, E. Ugur, G. Harrison, L. Grater, J. Wang, Z. Wang, L. Zeng, S. M. Park, L. Chen, P. Serles, R. A. Awni, B. Subedi, X. Zheng, C. Xiao, N. J. Podraza, T. Filleter, C. Liu, Y. Yang, J. M. Luther, S. De Wolf, M. G. Kanatzidis, Y. Yan, E. H. Sargent, *Nature* 2023, **613**, 676.

9. T. T. Li, J. Xu, R. X. Lin, S. Teale, H. J. Li, Z. Liu, C. Y. Duan, Q. Zhao, K. Xiao, P. Wu, B. Chen, S. Jiang, S. B. Xiong, H. W. Luo, S. S. Wan, L. D. Li, Q. Y. Bao, Y. X. Tian, X. P. Gao, J. Xie, E. H. Sargent, H. R. Tan, *Nat. Energy* 2023, **8**, 610.

10. J. Wen, Y. Zhao, P. Wu, Y. Liu, X. Zheng, R. Lin, S. Wan, K. Li, H. Luo, Y. Tian, L. Li, H. Tan, *Nat Commun* 2023, **14**, 7118.

11. S. Wu, Y. Yan, J. Yin, K. Jiang, F. Li, Z. Zeng, S.-W. Tsang, A. K. Y. Jen, *Nature Energy* 2024, **9**, 411-421.

12. Q. Jiang, J. Tong, R. A. Scheidt, X. Wang, A. E. Louks, Y. Xian, R. Tirawat, A. F. Palmstrom, M. P. Hautzinger, S. P. Harvey, S. Johnston, L. T. Schelhas, B. W. Larson, E. L. Warren, M. C. Beard, J. J. Berry, Y. Yan, K. Zhu, *Science* 2022, **378**, 1295.

13. J. Zhu, Y. Luo, R. He, C. Chen, Y. Wang, J. Luo, Z. Yi, J. Thiesbrummel, C. Wang, F. Lang, H. Lai, Y. Xu, J. Wang, Z. Zhang, W. Liang, G. Cui, S. Ren, X. Hao, H. Huang, Y. Wang, F. Yao, Q. Lin, L. Wu, J. Zhang, M. Stolterfoht, F. Fu, D. Zhao, *Nat. Energy* 2023, **8**, 714.

14. R. He, W. Wang, Z. Yi, F. Lang, C. Chen, J. Luo, J. Zhu, J. Thiesbrummel, S.

Shah, K. Wei, Y. Luo, C. Wang, H. Lai, H. Huang, J. Zhou, B. Zou, X. Yin, S. Ren, X. Hao, L. Wu, J. Zhang, J. Zhang, M. Stolterfoht, F. Fu, W. Tang, D. Zhao, *Nature* 2023, **618**, 80.

15. Y. Wang, R. Lin, C. Liu, X. Wang, C. Chosy, Y. Haruta, A. D. Bui, M. Li, H. Sun, X. Zheng, H. Luo, P. Wu, H. Gao, W. Sun, Y. Nie, H. Zhu, K. Zhou, H. T. Nguyen, X. Luo, L. Li, C. Xiao, M. I. Saidaminov, S. D. Stranks, L. Zhang, H. Tan, *Nature* 2024**,** 10.1038/s41586-024-08158-626.

16. Y. Pan, J. Wang, Z. Sun, J. Zhang, Z. Zhou, C. Shi, S. Liu, F. Ren, R. Chen, Y. Cai, et al. *Nat. Commun.* 2024, **15**, 7335.

17. Z. Zhang, W. Chen, X. Jiang, J. Cao, H. Yang, H. Chen, F. Yang, Y. Shen, H. Yang, Q. Cheng, et al. *Nat. Energy* 2024, **9**, 592-601.

18. X. Jiang, S. Qin, L. Meng, G. He, J. Zhang, Y. Wang, Y. Zhu, T. Zou, Y. Gong, Z. Chen, et al. Nature 2024, 10.1038/s41586-024-08160-y.